

Detection of HC¹⁸O⁺ in a protoplanetary disk: exploring oxygen isotope fractionation of CO

KENJI FURUYA,^{1,2} TAKASHI TSUKAGOSHI,^{1,2} CHUNHUA QI,³ HIDEKO NOMURA,¹ L. ILSEDORE CLEEVEs,⁴ SEOKHO LEE,¹ AND TOMOHIRO C. YOSHIDA^{5,1}

¹*National Astronomical Observatory of Japan, Osawa 2-21-1, Mitaka, Tokyo 181-8588, Japan*

²*These authors contributed equally to this work.*

³*Harvard-Smithsonian Center for Astrophysics 60 Garden Street Cambridge, MA 02138, USA*

⁴*Department of Astronomy, University of Virginia, Charlottesville, VA 22904, USA*

⁵*Department of Astronomical Science, The Graduate University for Advanced Studies (SOKENDAI), Osawa, Mitaka, Tokyo 181-8588, Japan*

(Received; Revised; Accepted)

Submitted to ApJ

ABSTRACT

The oxygen isotope fractionation scenario, which has been developed to explain the oxygen isotope anomaly in the solar system materials, predicts that CO gas is depleted in ¹⁸O in protoplanetary disks, where segregation between solids and gas inside disks had already occurred. Based on ALMA observations, we report the first detection of HC¹⁸O⁺(4–3) in a Class II protoplanetary disk (TW Hya). This detection allows us to explore the oxygen isotope fractionation of CO in the TW Hya disk from optically thin HCO⁺ isotopologues as a proxy of optically thicker CO isotopologues. Using the H¹³CO⁺(4–3) data previously obtained with SMA, we find that the H¹³CO⁺/HC¹⁸O⁺ ratio in the central $\lesssim 100$ au regions of the disk is 10.3 ± 3.2 . We construct a chemical model of the TW Hya disk with carbon and oxygen isotope fractionation chemistry, and estimate the conversion factor from H¹³CO⁺/HC¹⁸O⁺ to ¹³CO/C¹⁸O. With the conversion factor (= 0.8), the ¹³CO/C¹⁸O ratio is estimated to be 8.3 ± 2.6 , which is consistent with the elemental abundance ratio in the local ISM (8.1 ± 0.8) within error margin. Then there is no clear evidence of ¹⁸O depletion in CO gas of the disk, although we could not draw any robust conclusion due to uncertainties. In conclusion, optically thin lines of HCO⁺ isotopologues are useful tracers of CO isotopic ratios, which are hardly constrained directly from optically thick lines of CO isotopologues. Future higher sensitivity observations of H¹³CO⁺ and HC¹⁸O⁺ would be able to allow us to better constrain the oxygen fractionation in the disk.

Keywords: astrochemistry — protoplanetary disks — ISM: molecules

1. INTRODUCTION

Molecular isotope ratios, such as D/H ratio of water, are powerful tools to understand the origin of solar system materials and their possible chemical link with interstellar materials (e.g., Cleeves et al. 2014; Furuya et al. 2017). The element oxygen has three stable isotopes: ¹⁶O, ¹⁷O, and ¹⁸O. It has been well estab-

lished that the solar system materials, including chondrules, Ca-Al-rich inclusions (CAIs), and the Earth's ocean, are enriched in ¹⁷O and ¹⁸O compared to the Sun, and their oxygen isotope compositions show mass-independent variations (e.g., Tenner et al. 2018). Fe-O-S-bearing cosmic symplectites within Acfer 094 meteorite shows the most significant ^{17,18}O enrichment among the solar system materials; the ¹⁶O/¹⁷O and ¹⁶O/¹⁸O ratios are larger by 25 % compared to the Sun (Sakamoto et al. 2007).

The leading hypothesis to explain the oxygen isotope fractionation observed in the solar system materials is isotope-selective photodissociation of CO by ultraviolet (UV) photons, either in the parent molecular cloud or in

Corresponding author: Kenji Furuya

kenji.furuya@nao.ac.jp

Corresponding author: Takashi Tsukagoshi

Takashi.Tsukagoshi@nao.ac.jp

the protosolar disk, followed by the formation of $^{17,18}\text{O}$ -enriched water ice (e.g., Clayton 2002; Yurimoto & Kuramoto 2004; Lyons & Young 2005). Recent detailed study of CAIs suggests that the parent molecular cloud is the more favorable place for that chemistry (Krot et al. 2020). CO photodissociation is subject to self-shielding (i.e., CO itself can be the dominant absorber of dissociating UV radiation rather than dust grains). Because rarer isotopologues (e.g., C^{18}O and C^{17}O) are less abundant than ^{12}CO , they are not self-shielded until deeper into the cloud or the disk. This property makes CO photodissociation an isotope-selective process (e.g., Visser et al. 2009; Miotello et al. 2014). $^{17,18}\text{O}$ -enriched atomic oxygen is produced as the photodissociation product of CO, and can be converted into $^{17,18}\text{O}$ -enriched water ice. As a result, the three major oxygen reservoirs in star- and planet-forming regions, CO gas, H_2O ice, and refractory silicate, could have different isotope compositions, where, for example, (i) CO gas is depleted in $^{17,18}\text{O}$, (ii) H_2O ice is enriched in $^{17,18}\text{O}$, and (iii) silicate dust shows no fractionation. In our solar system, H_2O in cometary ice is enriched in ^{18}O , which is consistent with this scenario (e.g., Schroeder I et al. 2019; Altwegg et al. 2019). In the protosolar disk, dust grains coated with water ice could settle to the midplane and drift radially inward (i.e., segregating $^{17,18}\text{O}$ -rich solids and $^{17,18}\text{O}$ -poor gas inside the disk). When the icy dust grains across the snowline, water ice sublimates (e.g., Cuzzi & Zahnle 2004). The water vapor could react with silicates to make solid materials in the inner solar system enriched in ^{17}O and ^{18}O (e.g., Yurimoto & Kuramoto 2004; Yamamoto et al. 2018), which could be incorporated into planetasimals (asteroids/meteorites) and ultimately into planets.

The oxygen isotope fractionation scenarios outlined above has been favored to explain the oxygen isotope compositions in the solar system materials, but it remains unclear whether this evolution can occur in all star-forming regions or some specific factors are required. For example, based on the physico-chemical model of the collapsing proto-solar cloud, Lee et al. (2008) suggested that UV radiation field enhanced by a nearby massive star is necessary to explain the oxygen isotope compositions in the solar system materials. To address the question, studies of oxygen isotope fractionation in both star- and planet-forming regions are crucial. It is, however, not straightforward to constrain the oxygen isotope fractionation in Class II disks, because of the faint (or the non-detection of) H_2O emission (Hogerheijde et al. 2011; Du et al. 2017; van Dishoeck et al. 2021), and because $^{12}\text{C}^{16}\text{O}$ and $^{13}\text{C}^{16}\text{O}$ rotational lines are often optically thick (Schwarz et al.

2016; Huang et al. 2018). To the best of our knowledge, Smith et al. (2009) is the only study, which observationally constrains the oxygen isotope fractionation of CO in protoplanetary disks. They reported that the $^{12}\text{C}^{16}\text{O}/^{12}\text{C}^{18}\text{O}$ ratio in a disk in VVCra, a binary T Tauri star, is 690 ± 30 based on the observations of rovibrational absorption lines of the CO isotopologues. The derived $^{12}\text{C}^{16}\text{O}/^{12}\text{C}^{18}\text{O}$ ratio is higher than the elemental abundance ratio $[\text{O}^{16}]/[\text{O}^{18}]$ in the local ISM of 557 ± 30 (Wilson 1999), probably due to the isotope selective photodissociation of CO in the disk surface (Smith et al. 2009).

Here we report the first detection of HC^{18}O^+ in a Class II protoplanetary disk around a T Tauri star, TW Hya. The TW Hya disk is one of the most studied Class II disks in terms of both physical and chemical structures. With the previously detected optically thin H^{13}CO^+ emission (Qi et al. 2008), this detection allows us to constrain the oxygen isotope fractionation of CO in the TW Hya disk, using a $\text{H}^{13}\text{CO}^+/\text{HC}^{18}\text{O}^+$ ratio as a proxy of a $^{13}\text{CO}/\text{C}^{18}\text{O}$ ratio. According to previous studies (Schwarz et al. 2016; Huang et al. 2018), $\text{CO}(3-2)$ and $^{13}\text{CO}(3-2)$ transitions are optically thick in the entire disk. Even $^{18}\text{CO}(3-2)$ is optically thick in the inner disk (inside ~ 20 au; Zhang et al. 2017). Thus, it is hard to constrain the oxygen isotope ratio of CO in the TW Hya disk directly from the observations of CO isotopologues.

The TW Hya disk is an ideal lab to search for isotopic variations in C and O, as it is known to have a low CO and H_2O abundances, based on observations of these species and HD (e.g., Hogerheijde et al. 2011; Bergin et al. 2013; Zhang et al. 2019). The underabundance of volatile carbon and oxygen could be a consequence of dust evolution and segregation between solids and gas inside the disk (Du et al. 2015; Krijt et al. 2018). Then, the segregation of solids and gas are likely common process to cause the volatile evolution observed in the TW Hya disk and the oxygen isotope fractionation observed in the solar system materials. This makes the TW Hya disk an ideal place to test the oxygen isotope fractionation theory; if the oxygen fractionation mechanism is/was at work in the TW Hya disk as in the proto-solar disk, CO in TW Hya should be depleted in ^{18}O (and ^{17}O).

The rest of this paper is organized as follows. Section 2 summarizes the observational details and the data reduction procedure. Section 3 presents the observational data products and the disk-integrated $\text{H}^{13}\text{CO}^+/\text{HC}^{18}\text{O}^+$ ratio. In Section 4, we discuss the relation between the $^{13}\text{CO}/\text{C}^{18}\text{O}$ ratio and the $\text{H}^{13}\text{CO}^+/\text{HC}^{18}\text{O}^+$ ratio with the help of thermo-

chemical model of the TW Hya disk. The interpretation of our findings is discussed in Section 5.

2. OBSERVATIONS

We analyzed the ALMA archive data (ID:2016.1.00311.S) to search for the HC^{18}O^+ emission line from the protoplanetary disk around TW Hya. The TW Hya disk is almost face-on with the inclination of 7° and the distance from the earth is 59.5 pc (Gaia Collaboration et al. 2016). The data consisted of two execution blocks; observations with an array configuration of C40-1 on 2017 April 8 and C40-5 on May 21. The integration times for the execution blocks were 28.8 min and 47.8 min for C40-1 and C40-5, respectively. The Band 7 receiver system was employed to detect the continuum emission at 347 GHz and some molecular lines. The 14 spectral windows (SPWs) were used in the Frequency Division Mode, and one of which was tuned for detecting the $\text{HC}^{18}\text{O}^+(4-3)$ transition. The bandwidth and the channel spacing were 58.5938 MHz and 61.035 kHz, respectively, corresponding to a velocity resolution of 54 m s^{-1} . The line-free channels of the SPWs were used for detecting the continuum emission at Band 7, whose aggregate bandwidth was $\sim 1.8 \text{ GHz}$. A quasar J1037-2934 was used for the calibration of the complex gain of the visibilities as well as the calibration for the bandpass characteristics.

The visibility data were reduced and calibrated using the Common Astronomical Software Application package (McMullin et al. 2007). The pipeline script given by ALMA was applied for each execution block for the initial data flagging and the calibration for the bandpass characteristics, complex gain, and flux scaling. After the flagging of bad data manually, the molecular line and the continuum were separated using *uvcontsub*. The continuum emission was taken from the line-free channel in all the SPWs employed in this observation.

Before the imaging of the HC^{18}O^+ line, we first made a continuum map from the visibilities of two execution blocks for making a calibration table from the self-calibration. We created the dirty map for each execution block, and to concatenate two execution blocks the disk center was determined by a 2D Gaussian fitting to the bright part of the disk emission using *imfit*. After that, the center of the field of view was modified to the disk center by *fixvis*, and we concatenated two execution blocks using *concat* with a positional tolerance. Then, the CLEAN map of the dust emission was reconstructed from the concatenated visibilities using *tclean*. For the imaging, we used the Briggs weighting with a robust parameter of 0.5. We also employed the multiscale CLEAN algorithm with scale parameters of $[0, 0.2, 0.6] \text{ arcsec}$.

With the initial CLEAN map as a model, we applied the self-calibration for the continuum data. We first made a calibration table solved in phase for the whole part of each execution block, and then the solution intervals were shortened from 300, 60, and 6 seconds for the short baseline execution block and from 300, 180, and 120 seconds for the long baseline one with iteratively improving the model visibility by making the CLEAN map. After the phase-only self-calibration described above, we applied the self-calibration in amplitude with a solution interval of the whole part of each execution block. Finally, the beam size of the continuum CLEAN map was $0''.23 \times 0''.20$ with a position angle of $80^\circ.3$, and the sensitivity was $95 \mu\text{Jy beam}^{-1}$.

The HC^{18}O^+ emission line was imaged from the continuum-subtracted measurement set after applying the calibration table obtained by the self-calibration for the continuum emission. The CLEAN map was reconstructed using *tclean* with the Briggs weighting (robust=0.5). To improve the image sensitivity, we employed a uvtaper of 0.8 arcsec. The multiscale CLEAN was used with scale parameters of $[0, 0.85, 2.55] \text{ asec}$. The velocity width of the image cube was gridded to 0.06 km s^{-1} , which is almost comparable to the velocity resolution of the channels. The beam size of the CLEANed HC^{18}O^+ map was $1''.05 \times 0''.86$ with a position angle of $85^\circ.1$. The noise level of the channel map was $75.2 \text{ mJy beam}^{-1}$. The observed line properties are summarized in Table 1.

3. RESULTS

3.1. HC^{18}O^+ emission map and spectra

The $\text{HC}^{18}\text{O}^+(4-3)$ emission is associated with the protoplanetary disk of TW Hya as shown in Figure 1. The position angle of the velocity gradient is consistent with previous CO measurements (Teague et al. 2019), indicating that the HC^{18}O^+ emission traces the Kepler rotating gas disk. The emission peak is offset from the continuum peak and is slightly stronger on the west side; these features are also seen in the $\text{HCO}^+(3-2)$ emission in this disk (Cleeves et al. 2015). The peak intensity of HC^{18}O^+ is $>6 \sigma$, where $1\sigma = 3.1 \text{ mJy km s}^{-1}$ is the rms measured in the integrated intensity map.

The spatially integrated spectrum of $\text{HC}^{18}\text{O}^+(4-3)$ over the central $5'' \times 5''$ region is shown in Figure 2. The spectrum shows the characteristic double-peak structure due to the Keplerian rotation.

3.2. $\text{H}^{13}\text{CO}^+/\text{HC}^{18}\text{O}^+$ ratio

Previous studies have found that $\text{HCO}^+(4-3)$ emission in the disk is likely optically thick, while $\text{H}^{13}\text{CO}^+(4-3)$ emission is optically thin (Cleeves et al. 2015).

Table 1. Summary of observed lines

Transition	Rest Frequency (GHz)	E_u (K)	Beam (PA)	Flux $< 4.1'' \times 1.8''$ ^b (Jy km s ⁻¹)	Flux $< 5'' \times 5''$ ^c (Jy km s ⁻¹)	Reference
HC ¹⁸ O ⁺ (4-3)	340.6329780	40.87	1''.05 \times 0''.86 (85°.1)	0.07 \pm 0.01	0.14 \pm 0.01	This work
H ¹³ CO ⁺ (4-3)	346.9983381	41.63	4''.1 \times 1''.8 (3°.3 ^a)	0.76 \pm 0.16	1.8 \pm 0.2	Qi et al. (2008)

NOTE— ^aValue for the central $4.1'' \times 1.8''$ region. ^b Uncertainty does not include flux calibration uncertainty. The integrated flux of H¹³CO⁺(4-3) is slightly different from that presented in Qi et al. (2008, 0.61 Jy km s⁻¹), because we recalculated it using the same procedure as the calculation of the HC¹⁸O⁺(4-3) integrated flux. ^c Uncertainty does not include flux calibration uncertainty.

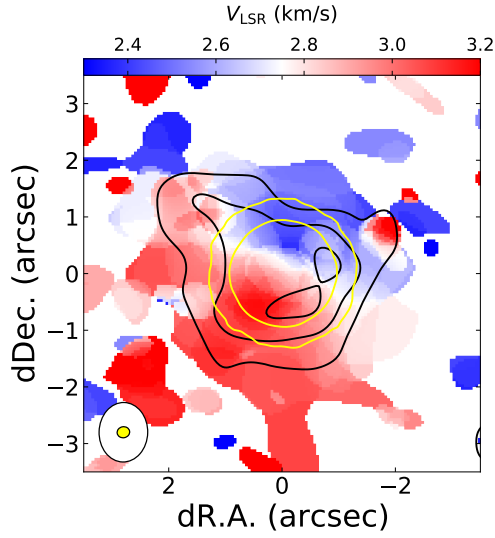


Figure 1. Map of the HC¹⁸O⁺(4-3) emission from the protoplanetary disk around TW Hya. The color scale indicates the weighted-mean velocity map. The integrated intensity from 2.3 to 3.5 km s⁻¹ is shown by the black contour. The contour interval is 2σ starting from 2σ , where $1\sigma = 3.1$ mJy km s⁻¹. The yellow contour represents the 10 and 100σ boundaries of the continuum emission, where $1\sigma = 92$ μ Jy km s⁻¹. The ellipse at the bottom-left corner denotes the beam size of the map, in which the HC¹⁸O⁺ is shown in white and the continuum is in yellow, respectively.

H¹³CO⁺(4-3) emission at 347 GHz was detected toward the TW Hya disk in the SMA observations with a beam of $4.1'' \times 1.8''$ (Qi et al. 2008). We checked the ALMA archive and confirmed that there is no available data for H¹³CO⁺(4-3) and the other transitions of H¹³CO⁺. Here we derive the H¹³CO⁺/HC¹⁸O⁺ ratio in the disk using the H¹³CO⁺(4-3) data obtained with SMA and its interpretation will be discussed in the following sections.

Table 1 lists the total integrated intensities of HC¹⁸O⁺(4-3) and H¹³CO⁺(4-3) within the central $4.1'' \times 1.8''$ region and across the entire HC¹⁸O⁺ disk (within a radius of $2.5''$). The total integrated intensities in the central $4.1'' \times 1.8''$ region are converted

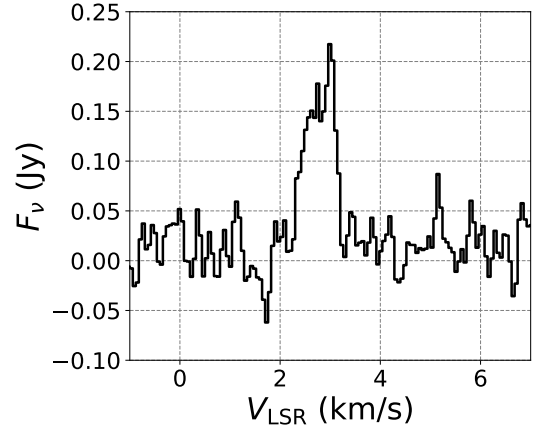


Figure 2. Spectrum of the flux density in HC¹⁸O(4-3) integrated over the central $5'' \times 5''$ box region.

into column densities using Eq. 82 in Mangum & Shirley (2015), assuming LTE and optically thin conditions. The parameters of the observed transitions were taken from the Cologne Database for Molecular Spectroscopy (Müller et al. 2001, 2005). Assuming that excitation temperature (T_{ex}) is 30 K, which is a typical temperature of warm molecular layers (e.g., Aikawa et al. 2002, see also Section 4), the column densities of H¹³CO⁺ and HC¹⁸O⁺ in the central $4.1'' \times 1.8''$ region are $(5.8 \pm 1.5) \times 10^{11}$ cm⁻² and $(5.6 \pm 1.0) \times 10^{10}$ cm⁻², respectively. The uncertainty includes 15 % flux calibration uncertainty for the SMA data (Qi et al. 2008) and 10 % flux calibration uncertainty for the ALMA data. The flux calibration uncertainties do not significantly affect the uncertainties in the derived column densities, because the RMS noises are larger than the calibration uncertainties. If T_{ex} is assumed to be 20 K, the estimated column densities become slightly higher: $(7.8 \pm 2.0) \times 10^{11}$ cm⁻² for H¹³CO⁺ and $(7.5 \pm 1.3) \times 10^{10}$ cm⁻² for HC¹⁸O⁺.

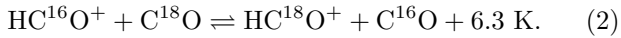
Then the H¹³CO⁺/HC¹⁸O⁺ column density ratio in the central $4.1'' \times 1.8''$ region is estimated to be 10.3 ± 3.2 , which is consistent with the elemental abundance

ratio $[^{13}\text{C}][^{16}\text{O}]/([^{12}\text{C}][^{18}\text{O}])$ in the local ISM of 8.1 ± 0.8 (Wilson 1999) within error margin. Note that the column density ratio is not sensitive to the choice of the excitation temperature, because the difference in upper state energy is less than 1 K between H¹³CO⁺(4–3) and HC¹⁸O⁺(4–3) (Table 1).

We also calculate the H¹³CO⁺/HC¹⁸O⁺ column density ratio in the entire HC¹⁸O⁺ disk (within a radius of 2.5'') in a similar way. The ratio is evaluated to be 12.5 ± 2.8 , which is consistent with that in the central $4.1'' \times 1.8''$ region within error margin (10.3 ± 3.2). Then, in the rest of this paper, we discuss the H¹³CO⁺/HC¹⁸O⁺ column density ratio in the central $4.1'' \times 1.8''$ (240 au \times 110 au) region.

4. DISK CHEMISTRY MODELING

In this section, we discuss the relation between the $^{13}\text{CO}/\text{C}^{18}\text{O}$ ratio and the H¹³CO⁺/HC¹⁸O⁺ ratio. As HCO⁺ is formed by the proton transfer reaction, $\text{CO} + \text{H}_3^+ \rightarrow \text{HCO}^+ + \text{H}_2$, and is destroyed by the dissociative recombination reactions with electrons, $\text{HCO}^+ + \text{e}^- \rightarrow \text{CO} + \text{H}$, one may expect that the isotopic ratios of HCO⁺ directly reflect those of CO. According to previous astrochemical models in molecular clouds and protoplanetary disks (e.g., Langer et al. 1984; Woods & Willacy 2009; Furuya et al. 2011), this is not always the case; the isotopic ratios of HCO⁺ are modified by isotope exchange reactions. CO and HCO⁺ exchange carbon and oxygen isotopes via the following reactions (Mladenović & Roueff 2014, 2017; Loison et al. 2019):



The forward reactions are exothermic, while the reverse reactions are slightly endothermic due to the difference in the zero point energy among the different isotopologues (Mladenović & Roueff 2017). Woods & Willacy (2009) found that the HCO⁺/H¹³CO⁺ abundance ratio deviates from CO/¹³CO, and is determined by the balance between the forward and backward directions of Reaction 1 in their disk chemical model. Note that the gas-phase CO abundance is the canonical value ($\sim 10^{-4}$) in the disk model by Woods & Willacy (2009), while in the TW Hya disk, it is lower than the canonical value by a factor of >10 , based on the observations of HD and CO isotopologues (e.g., Favre et al. 2013). Then it remains unclear whether the isotope exchange reactions are efficient enough to determine the isotopic ratios of HCO⁺ in the TW Hya disk.

Considering the above mentioned reactions and assuming the balance between the formation and destruction of the HCO⁺ isotopologues, the relation between

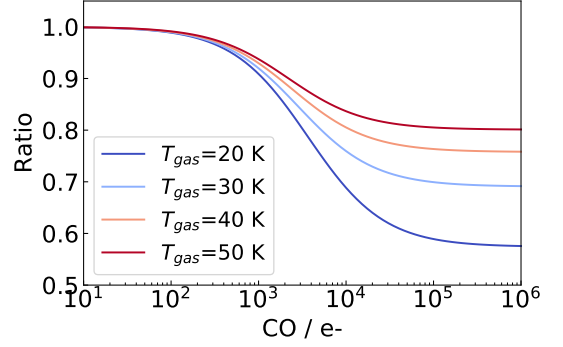


Figure 3. Ratio of $^{13}\text{CO}/\text{C}^{18}\text{O}$ to $\text{H}^{13}\text{CO}^+/\text{HC}^{18}\text{O}^+$ as a function of the abundance ratio between CO and electrons, varying the gas temperature. See the text for details.

$^{13}\text{CO}/\text{C}^{18}\text{O}$ and $\text{H}^{13}\text{CO}^+/\text{HC}^{18}\text{O}^+$ is given by

$$\frac{x(^{13}\text{CO})}{x(\text{C}^{18}\text{O})} = \frac{k_{\text{ex}1}x(\text{CO}) + k_{\text{rec}}x(\text{e}^-)}{k_{\text{ex}2}x(\text{CO}) + k_{\text{rec}}x(\text{e}^-)} \times \frac{x(\text{H}^{13}\text{CO}^+)}{x(\text{HC}^{18}\text{O}^+)}, \quad (3)$$

where $x(i)$ is the abundance of species i , k_{rec} is the rate coefficient of the electron recombination of the HCO⁺ isotopologues, and $k_{\text{ex}1}$ and $k_{\text{ex}2}$ are the rate coefficient in the reverse direction of Reaction 1 and Reaction 2, respectively. If both Reactions 1 and 2 are in chemical equilibrium, i.e., when the HCO⁺ destruction by the dissociative recombination with electrons is much slower than the isotope exchange reactions, Eq. 3 is reduced to be $x(^{13}\text{CO})/x(\text{C}^{18}\text{O}) = x(\text{H}^{13}\text{CO}^+)/x(\text{HC}^{18}\text{O}^+) \times \exp(-11.1 \text{ K}/T_{\text{gas}})$. Figure 3 visualizes the ratio of $x(^{13}\text{CO})/x(\text{C}^{18}\text{O})$ to $x(\text{H}^{13}\text{CO}^+)/x(\text{HC}^{18}\text{O}^+)$ as functions of $x(\text{CO})/x(\text{e}^-)$.

It is difficult to constrain the $x(\text{CO})/x(\text{e}^-)$ ratio from observations, because several species, such as H_3^+ , HCO^+ , N_2H^+ , S^+ , and C^+ , would contribute to the total charge in the warm molecular layer (e.g., Aikawa et al. 2015; Teague et al. 2015). However, the $x(\text{CO})/x(\text{HCO}^+)$ ratio would provide a rough upper limit of the $x(\text{CO})/x(\text{e}^-)$ ratio in the warm molecular layer. Assuming the HCO⁺/H¹³CO⁺ ratio of 69, the averaged HCO⁺ column density in the central 240 au \times 110 au ($4.1'' \times 1.8''$) regions is $\sim 4 \times 10^{13} \text{ cm}^{-2}$. According to Zhang et al. (2019), the CO column density at $r = 60 - 120 \text{ au}$ is $\sim 10^{17} - 10^{18} \text{ cm}^{-2}$. Then the $x(\text{CO})/x(\text{HCO}^+)$ ratio is roughly estimated to be $\sim 3 \times 10^3 - 3 \times 10^4$. The HCO⁺ isotopologues emission would mainly originate from the regions at $T_{\text{gas}} \gtrsim 20 \text{ K}$ in the TW Hya disk, because HCO⁺ is formed from CO and CO is frozen out onto dust grains at $\lesssim 20 \text{ K}$. Taken together, we expect that the $^{13}\text{CO}/\text{C}^{18}\text{O}$ ratio is 70–100 % of the H¹³CO⁺/HC¹⁸O⁺ ratio.

4.1. Model description

To explore the relation between $x(^{13}\text{CO})/x(\text{C}^{18}\text{O})$ and $x(\text{H}^{13}\text{CO}^+)/x(\text{HC}^{18}\text{O}^+)$ in the TW Hya disk in more details, we construct a physical and chemical model of the TW Hya disk with carbon and oxygen isotope fractionation chemistry. The dust and gas density profiles in the disk are taken from the TW Hya disk model developed in Cleeves et al. (2015). The total gas mass is $0.04 M_{\odot}$ and the dust-to-gas mass ratio is 0.01 as a whole. Two populations of dust grains are considered: the small dust population with radii of $0.005 - 1 \mu\text{m}$ and the large dust population with radii of $0.005 \mu\text{m} - 1 \text{mm}$. The fraction of mass in the large dust population is set to be $f = 0.9$. Both populations follow a power law size distribution with the index of -3.5. The small dust population is assumed to be coupled with gas, while the large dust population is concentrated near the midplane and its scale height is a factor of five smaller than that of gas (Cleeves et al. 2015).

The dust temperature in the disk is calculated using the radiative transfer code RADMC-3D (Dullemond et al. 2012). The input UV and X-ray spectra of TW Hya are taken from Dionatos et al. (2019), and they are added to a Black body component with the effective temperature of 4110 K (Andrews et al. 2012). The local UV radiation and X-ray radiation fields inside the disk are also calculated with RADMC-3D, considering both absorption and scattering. Our model does not consider the resonant scattering of $\text{Ly}\alpha$ photons, which dominates the stellar FUV flux (Herczeg et al. 2002), by atomic H (Bethell & Bergin 2011a). This simplification would not affect our results significantly, as CO is not dissociated by $\text{Ly}\alpha$. The dust opacity for UV and longer wavelengths is calculated with `dsharp_opac` package from Birnstiel et al. (2018). The gas and dust opacities for X-rays are calculated with the method proposed by Bethell & Bergin (2011b) with the X-ray absorption and scattering cross sections taken from `xraylib` library (Brunetti et al. 2004; Schoonjans et al. 2011).

The gas temperature and chemical composition of the disk is calculated by integrating the energy equation and chemical rate equations simultaneously for 1 Myr, which is shorter than the age of TW Hya ($8 \pm 4 \text{ Myr}$; Donaldson et al. 2016), but long enough for the abundances of CO and HCO^+ isotopologues to reach steady-state in our model. The use of a shorter time than the age of TW Hya would be reasonable, as the current physical structure adopted represents the TW Hya disk today and not during the disk's entire 8 Myr evolution. As heating and cooling processes, photoelectric heating, X-ray and cosmic-ray heating, heating by the H_2 formation and photodissociation, the energy exchange between gas

and dust particles due to collisions, and line cooling by atoms and molecules (H, H_2 , C, O, CO, OH, and H_2O) are considered (e.g., Tielens 2005). The disk physical structures are shown in Appendix.

The chemical network used in this work is based on that in Furuya & Aikawa (2014), which includes gas-phase reactions, interaction between gas and (icy) grain surfaces, and grain surface reactions. The network is extended to include mono- ^{13}C and mono- ^{18}O species (species with both ^{13}C and ^{18}O , e.g., $^{13}\text{C}^{18}\text{O}$, are included), and carbon and oxygen isotope exchange reactions (Roueff et al. 2015; Mladenović & Roueff 2017; Loison et al. 2019, 2020). UV photodissociation/photoionization rates are calculated by convolving the local radiation field and the photodissociation/photoionization cross sections (Heays et al. 2017). The self-shielding and mutual shielding factors for the photodissociation of CO isotopologues are taken from Visser et al. (2009). The column densities for calculating the shielding factors are evaluated by the minimum of the inward/upward column. This method is computationally cheap and often adopted in the literature (e.g., Miotello et al. 2014), but can underestimate the effect of self-shielding (see the appendix of Lee et al. 2021). X-ray chemistry is calculated in the same way as in Furuya et al. (2013). The binding energy of CO is set to be 855 K (Öberg et al. 2005). The cosmic-ray ionization rate is set to be 10^{-18} s^{-1} .

Table 2 lists initial molecular abundances for the disk model. As shown by previous observations and the analysis based on thermo-chemical disk models, the CO abundance is low in the warm molecular layers ($>20 \text{ K}$) and the C/O ratio is higher than unity in the TW Hya disk (e.g., Bergin et al. 2016; Kama et al. 2016; Zhang et al. 2019; Cleeves et al. 2021; Nomura et al. 2021). In our model, the elemental carbon abundance is 1.4×10^{-6} with the C/O ratio of 1.5. As long as $\text{C/O} > 1$, our model results are not sensitive to the choice of the C/O ratio, as the abundances of CO and HCO^+ are regulated by the oxygen abundance rather than the carbon abundance. Initially, the $^{12}\text{C}/^{13}\text{C}$ and $^{16}\text{O}/^{18}\text{O}$ ratios for all the species are set to be 69 and 557, respectively (Wilson 1999), i.e., there is no fractionation at the beginning of the simulations.

4.2. Model results

The upper panels of Figure 4 shows the spatial distributions of fractional abundances of CO and HCO^+ with respect to hydrogen nuclei. CO is abundant ($\sim 10^{-6}$) in the warm molecular layers ($\gtrsim 20 \text{ K}$). Above the warm molecular layers, CO is efficiently destroyed by UV photodissociation, while below the warm molecular layers,

Table 2. Initial abundances with respect to hydrogen nuclei.

Species	Abundance	Species	Abundance
H_2	0.5	N	2.8(-5)
He	9.55(-2)	S^+	8.0(-8)
CO	1.4(-6)	Si^+	8.0(-9)
C	2.2(-6)	Fe^+	3.0(-9)
H_2O	1.0(-6)	Na^+	2.0(-9)
N_2	1.4(-5)	Mg^+	7.0(-9)

NOTE— $a(-b)$ means $a \times 10^{-b}$.

CO is frozen out onto dust grains. The spatial distribution of HCO^+ basically follows that of CO, as it is formed by $\text{CO} + \text{H}_3^+$. The dominant ionization sources in the regions where HCO^+ is abundant are X-rays rather than cosmic-rays in our model, being consistent with the model in [Cleeves et al. \(2015\)](#).

The lower panels of Figure 4 shows the $^{13}\text{CO}/\text{C}^{18}\text{O}$ abundance ratio and the $\text{H}^{13}\text{CO}^+/\text{HC}^{18}\text{O}^+$ abundance ratio. The $^{13}\text{CO}/\text{C}^{18}\text{O}$ ratio does not show significant fractionation except for the thin layer ($z/R \sim 0.2 - 0.3$), where the ratio is higher than the elemental abundance ratio. In these regions, C^{18}O is not self-shielded, while ^{13}CO is, resulting in the overabundance of ^{13}CO with respect to C^{18}O . Indeed, the overabundance of ^{13}CO with respect to C^{18}O has been observed in molecular clouds illuminated by UV photons from nearby stars (e.g., [Shimajiri et al. 2014](#)). The $\text{H}^{13}\text{CO}^+/\text{HC}^{18}\text{O}^+$ ratio is similar to the $^{13}\text{CO}/\text{C}^{18}\text{O}$ ratio except for regions at $z/R \sim 0.1 - 0.2$, where the abundance ratio between CO and electrons is $\sim 10^4 - 10^5$, and Reactions 1 and 2 modify the $\text{H}^{13}\text{CO}^+/\text{HC}^{18}\text{O}^+$ ratio (see Figure 3).

The left panel of Figure 5 shows radial profiles of the column densities of HCO^+ isotopologues. The column densities of H^{13}CO^+ and HC^{18}O^+ in our model reasonably well reproduce those derived from the observations assuming $T_{\text{ex}} = 30$ K and the optically thin emissions. We checked the optical depth of the $\text{H}^{13}\text{CO}^+(4-3)$ line for a slab of H_2 and H^{13}CO^+ gas using the Radex code ([van der Tak et al. 2007](#)). The peak H^{13}CO^+ column density in our model is $7 \times 10^{11} \text{ cm}^{-2}$. Assuming an H_2 density of 10^9 cm^{-3} , the kinetic temperature of 30 K, linewidth of 0.13 km/s due to the thermal broadening, the H^{13}CO^+ column density of $7 \times 10^{11} \text{ cm}^{-2}$ corresponds to the optical depth of ~ 0.48 for the $\text{H}^{13}\text{CO}^+(4-3)$ line. Then as claimed by [Cleeves et al. \(2015\)](#), the $\text{H}^{13}\text{CO}^+(4-3)$ line is likely optically thin in the TW Hya disk.

The right panel of Figure 5 shows radial profiles of $^{13}\text{CO}/\text{C}^{18}\text{O}$ column density ratio and

$\text{H}^{13}\text{CO}^+/\text{HC}^{18}\text{O}^+$ column density ratio. The $^{13}\text{CO}/\text{C}^{18}\text{O}$ column density ratio is very close to the elemental abundance ratio of 8.1, because the isotope selective photodissociation of CO is significant only in limited regions. This result is qualitatively consistent with the results of generic disk models in [Miotello et al. \(2014, 2016\)](#), who found that the impact of isotope selective photodissociation of CO is less significant in more massive disks with smaller CO abundance. The $\text{H}^{13}\text{CO}^+/\text{HC}^{18}\text{O}^+$ ratio is lower than $^{13}\text{CO}/\text{C}^{18}\text{O}$ at all the radii in our disk model by a factor of ~ 0.8 . Then in the rest of this paper, we assume the following relation from these models; $^{13}\text{CO}/\text{C}^{18}\text{O} = 0.8 \times (\text{H}^{13}\text{CO}^+/\text{HC}^{18}\text{O}^+)$.

5. DISCUSSION & CONCLUSION

Given TW Hya's proximity, we can compare the isotopic ratio to the local ISM ratio of $^{13}\text{C}/^{12}\text{C}$ of 8.1 ± 0.8 ([Wilson 1999](#)). Based on our measurement and model-derived correction factor, we estimate the $^{13}\text{CO}/\text{C}^{18}\text{O}$ ratio in the TW Hya disk ratio to be 8.3 ± 2.6 . The $^{13}\text{CO}/\text{C}^{18}\text{O}$ ratio is consistent with the elemental ratio in the local ISM.

It would be instructive to check how the $^{13}\text{CO}/\text{C}^{18}\text{O}$ column density ratio estimated from $\text{H}^{13}\text{CO}^+/\text{HC}^{18}\text{O}^+$ is compared with the $^{13}\text{CO}/\text{C}^{18}\text{O}$ intensity ratio observed in the disk. For this purpose, we use the ALMA data targeting $^{13}\text{CO}(3-2)$ and $\text{C}^{18}\text{O}(3-2)$ in the TW Hya disk with the spatial resolution of ~ 9 au, presented in [Nomura et al. \(2021\)](#). The top and bottom panels of Figure 6 show the radial profiles of the integrated intensity of ^{13}CO and C^{18}O and the intensity ratio of $^{13}\text{CO}/\text{C}^{18}\text{O}$, respectively. The $^{13}\text{CO}/\text{C}^{18}\text{O}$ intensity ratio is as low as three at $R < 80$ au, indicating the ^{13}CO emission is likely optically thick as suggested by previous studies ([Schwarz et al. 2016](#)). At optically thinner region beyond 80 au, the ratio may be larger than ~ 4 , but we cannot constrain the intensity ratio well due to the weak C^{18}O emission.

Based on the $\text{C}^{18}\text{O}(3-2)$ and $^{13}\text{C}^{18}\text{O}(3-2)$ observations, [Zhang et al. \(2017\)](#) tentatively found that the $\text{CO}/^{13}\text{CO}$ ratio in the TW Hya disk is 40^{+9}_{-6} , which is lower than the $^{12}\text{C}/^{13}\text{C}$ ratio of 69 in the local ISM ([Wilson 1999](#)). The authors noted that higher sensitivity observations are needed to confirm this ratio, because the ratio was derived from the disk regions where the S/N ratio of $^{13}\text{C}^{18}\text{O}(3-2)$ was not high. Our model predicts that bulk CO is slightly enriched in ^{13}C due to the isotope exchange reaction, $^{13}\text{C}^+ + \text{CO} \rightleftharpoons \text{C}^+ + ^{13}\text{CO} + 35 \text{ K}$ (e.g., [Langer et al. 1984](#)); the $^{12}\text{CO}/^{13}\text{CO}$ column density ratio in our model is 62–69, depending on radius. If we assume that $^{12}\text{CO}/^{13}\text{CO} = 69$, the

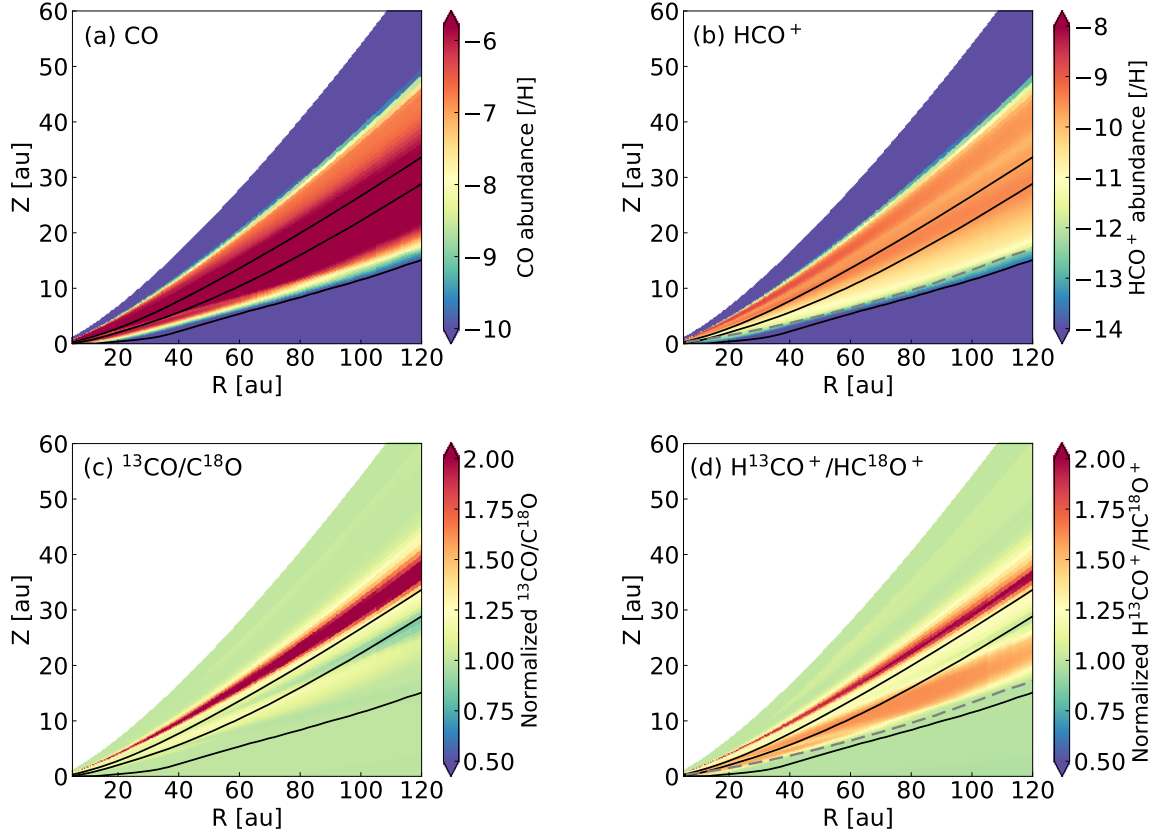


Figure 4. Spatial distributions of fractional abundances of CO (panel a) and HCO^+ (panel b) with respect to hydrogen nuclei, and the normalized abundances ratios of $^{13}\text{CO}/\text{C}^{18}\text{O}$ (panel c) and $\text{H}^{13}\text{CO}^+/\text{HC}^{18}\text{O}^+$ (panel d) with respect to the elemental abundance ratio of 8.1 in the disk model. Black lines depict the positions where the gas temperature is equal to 20 K, 30 K, and 40 K. Gray dashed lines in the panels b and d depict the positions where the X-ray ionization rate is equal to the cosmic-ray ionization rate (10^{-18} s^{-1}).

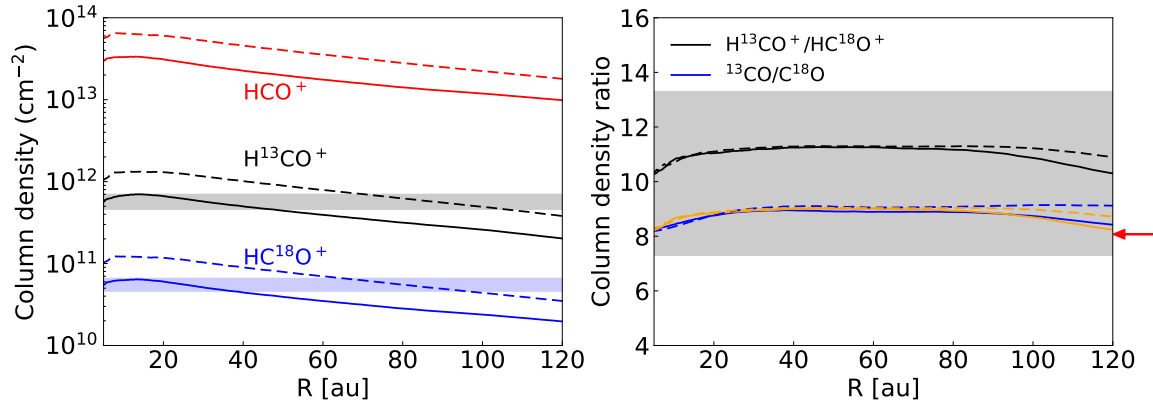


Figure 5. Left) Radial profiles of the column densities of HCO^+ isotopologues in our disk models. Right) Radial profiles of $^{13}\text{CO}/\text{C}^{18}\text{O}$ column density ratio (blue) and $\text{H}^{13}\text{CO}^+/\text{HC}^{18}\text{O}^+$ column density ratio (black) in the disk models. Orange line in the right panel represents the $^{13}\text{CO}/\text{C}^{18}\text{O}$ column density ratio multiplied by a factor of 0.8. Solid lines show the results of our fiducial model, while dashed lines show the results of the model with five times higher stellar X-ray flux. Areas represent the observationally derived values in the TW Hya disk assuming $T_{\text{ex}} = 30 \text{ K}$. In the right panel, red arrow in the right margin shows the elemental $[^{13}\text{C}]/[^{16}\text{O}]$ ratio adopted in the disk model.

$\text{CO}/\text{C}^{18}\text{O}$ ratio is estimated to be 390–750. If we assume

the $^{12}\text{CO}/^{13}\text{CO}$ ratio derived by Zhang et al. (2017), the estimated $\text{CO}/\text{C}^{18}\text{O}$ ratio is lower than 530.

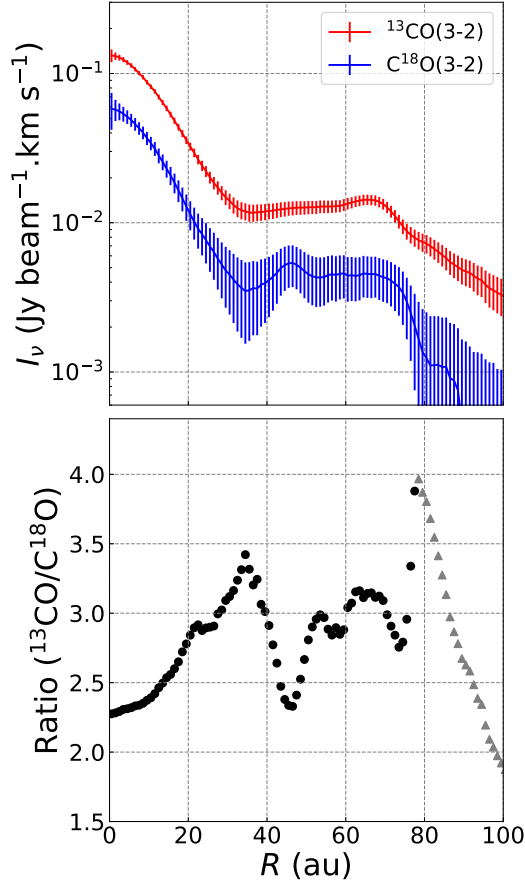


Figure 6. (Top) Radial profiles of the integrated intensity in $^{13}\text{CO}(3-2)$ and $\text{C}^{18}\text{O}(3-2)$ (Nomura et al. 2021). (Bottom) Ratio of the $^{13}\text{CO}(3-2)/\text{C}^{18}\text{O}(3-2)$ integrated intensities. The ratio is estimated for the C^{18}O signals above 1.5σ and shown in black points. The gray triangles indicate the lower limit of the ratio calculated from the 1.5σ value of the C^{18}O emission.

Although the $\text{CO}/\text{C}^{18}\text{O}$ ratio in the proto-solar disk is unknown, there are some constraints on the $\text{H}_2^{16}\text{O}/\text{H}_2^{18}\text{O}$ ratio. Evidence for primordial heavy isotope enriched H_2O ice comes from Fe-O-S-bearing cosmic symplectites within Acfer 094 meteorite, which shows 25 % enrichment of ^{18}O (and ^{17}O) compared to the Solar wind (Sakamoto et al. 2007), corresponding to $\text{H}_2^{16}\text{O}/\text{H}_2^{18}\text{O} = 400$. Cometary water ice shows variations in $\text{H}_2^{16}\text{O}/\text{H}_2^{18}\text{O}$, ranging 400-500 (Bockelée-Morvan et al. 2015; Altwegg et al. 2019). Then, assuming the $\text{H}_2\text{O}/\text{CO}$ abundance ratio of unity at the moment when oxygen isotope fractionation was implemented, CO should be depleted in ^{18}O (and ^{17}O) by up to 25 % compared to the Solar wind, corresponding to $\text{CO}/\text{C}^{18}\text{O} = 660$. The disk chemical model with turbulent mixing (Lyons & Young 2005) predicted that CO could be depleted in ^{18}O by up to ~ 60 % compared to the Solar

wind, corresponding to $\text{CO}/\text{C}^{18}\text{O} = 850$. Note that the $^{16}\text{O}/^{18}\text{O}$ ratio in the Solar wind and that in the local ISM is similar (530 versus 557 ± 30).

Taken together, at this moment, there is no clear evidence of ^{18}O depletion in the observable CO gas in the central 100 au regions of the TW Hya disk. However, there are uncertainties, including the large error in the $\text{H}^{13}\text{CO}^+/\text{HC}^{18}\text{O}^+$ ratio (and thus $^{13}\text{CO}/\text{C}^{18}\text{O}$), and we cannot draw any robust conclusions yet. If confirmed, this implies that the material evolution in the TW Hya disk is different from that experienced in the proto-solar disk for some reason. One possibility might be the different birth environment (the TW Hya disk is in quiescent regions, while the sun was likely born in a cluster region), i.e., external UV radiation field might be the crucial parameter for the oxygen isotope fractionation scenario. Future higher sensitivity observations of HCO^+ isotopologues are necessary for better constraining the oxygen isotope ratio of CO gas in the TW Hya disk. The confirmation of the low $^{12}\text{CO}/^{13}\text{CO}$ ratio suggested by Zhang et al. (2017) is also crucial for constraining the oxygen isotope ratio.

Finally, we note that the possible effect of stellar X-ray variability on the above discussion. Cleaves et al. (2017) found that $\text{H}^{13}\text{CO}^+(3-2)$ line intensity from the disk around a Tauri star, IM Lup, measured in May 2015 is brighter by a factor of ~ 2 compared to that in January 2015, due to X-ray flare events. As the HC^{18}O^+ data and H^{13}CO^+ data used in this work were taken at a different epoch, we can not rule out the possibility that the $\text{H}^{13}\text{CO}^+/\text{HC}^{18}\text{O}^+$ ratio, and thus the $^{13}\text{CO}/\text{C}^{18}\text{O}$ ratio derived in this work, is affected by stellar X-ray variability. In order to check the effect of X-ray variability quickly, we reran our disk model with five times higher stellar X-ray flux. We confirmed that the column densities of the HCO^+ isotopologues are increased by a factor of $\sim \sqrt{5}$, because the main ionization source is X-rays in the regions where HCO^+ is abundant in our model, and because the abundance of major molecular ions, such as HCO^+ , is proportional to $\sqrt{\xi}$, where ξ is the ionization rate (e.g., Aikawa et al. 2015). On the other hand, the column density ratios of $\text{H}^{13}\text{CO}^+/\text{HC}^{18}\text{O}^+$ and $^{13}\text{CO}^+/\text{C}^{18}\text{O}$ do not change significantly (the dashed lines in Figure 5). Then, simultaneous observations of HCO^+ isotopologues would be able to eliminate the possible effect of X-ray variability on the measurements of the isotopic ratios of HCO^+ and thus those of CO.

ACKNOWLEDGMENTS

This work makes use of the following public ALMA archive data: ADS/JAO.ALMA#2016.1.00311.S. ALMA is a partnership of ESO (representing its member states), NSF (USA) and NINS (Japan), together with NRC (Canada), MOST and ASIAA (Taiwan), and KASI (Republic of Korea), in cooperation with the Republic of Chile. A part of the data analysis was carried out on the common-use data analysis computer system at the Astronomy Data Center of NAOJ. Numerical computations were in part carried out on PC cluster at Center for Computational Astrophysics, NAOJ. K.F. is supported by JSPS KAKENHI Grant numbers 20H05847, 21H04487, and 21K13967. T.T. is supported by JSPS KAKENHI Grant number 20K04017.

APPENDIX

A. DISK PHYSICAL STRUCTURE

Figure 7 shows the disk physical structures in our model.

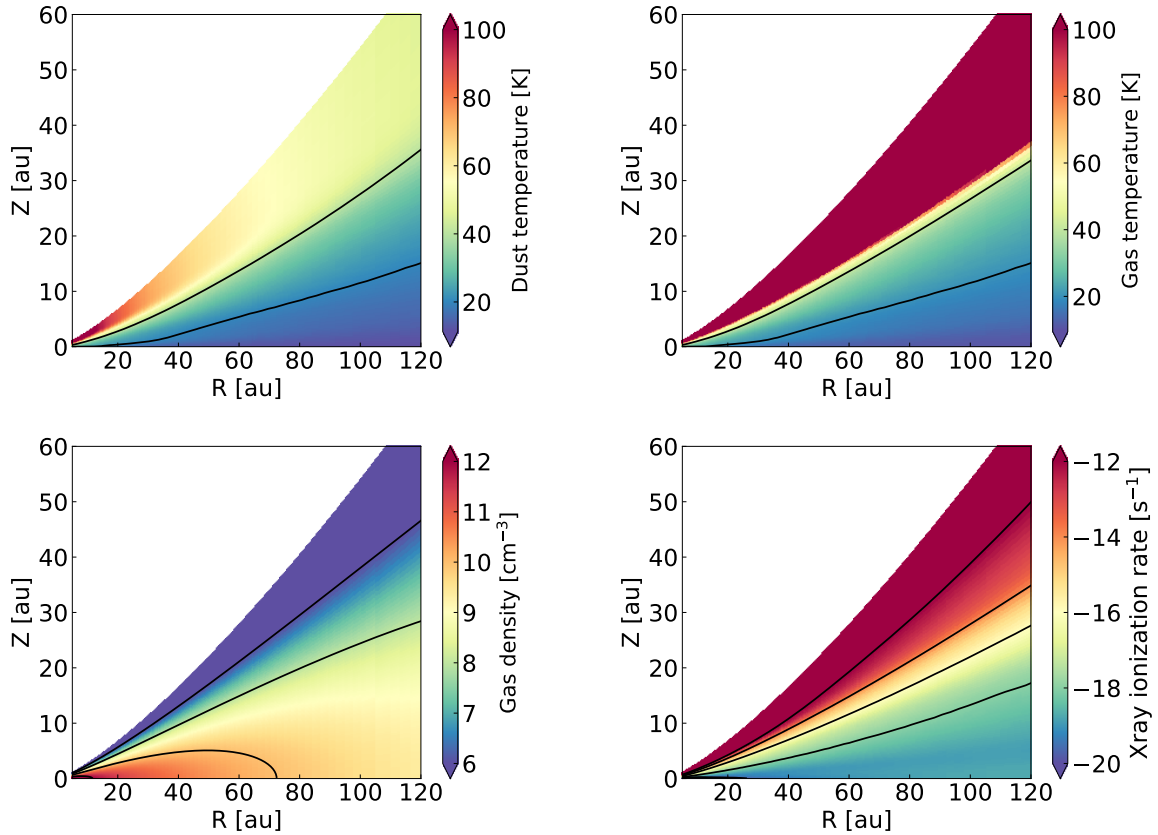


Figure 7. Spatial distributions of dust temperature, gas temperature, gas density, and X-ray ionization rate in our disk model.

REFERENCES

- Aikawa, Y., Furuya, K., Nomura, H., & Qi, C. 2015, *ApJ*, 807, 120, doi: [10.1088/0004-637X/807/2/120](https://doi.org/10.1088/0004-637X/807/2/120)
- Aikawa, Y., van Zadelhoff, G. J., van Dishoeck, E. F., & Herbst, E. 2002, *A&A*, 386, 622, doi: [10.1051/0004-6361:20020037](https://doi.org/10.1051/0004-6361:20020037)
- Altwegg, K., Balsiger, H., & Fuselier, S. A. 2019, *ARA&A*, 57, 113, doi: [10.1146/annurev-astro-091918-104409](https://doi.org/10.1146/annurev-astro-091918-104409)
- Andrews, S. M., Wilner, D. J., Hughes, A. M., et al. 2012, *ApJ*, 744, 162, doi: [10.1088/0004-637X/744/2/162](https://doi.org/10.1088/0004-637X/744/2/162)
- Bergin, E. A., Du, F., Cleeves, L. I., et al. 2016, *ApJ*, 831, 101, doi: [10.3847/0004-637X/831/1/101](https://doi.org/10.3847/0004-637X/831/1/101)
- Bergin, E. A., Cleeves, L. I., Gorti, U., et al. 2013, *Nature*, 493, 644, doi: [10.1038/nature11805](https://doi.org/10.1038/nature11805)
- Bethell, T. J., & Bergin, E. A. 2011a, *ApJ*, 739, 78, doi: [10.1088/0004-637X/739/2/78](https://doi.org/10.1088/0004-637X/739/2/78)
- . 2011b, *ApJ*, 740, 7, doi: [10.1088/0004-637X/740/1/7](https://doi.org/10.1088/0004-637X/740/1/7)
- Birnstiel, T., Dullemond, C. P., Zhu, Z., et al. 2018, *ApJL*, 869, L45, doi: [10.3847/2041-8213/aaf743](https://doi.org/10.3847/2041-8213/aaf743)
- Bockelée-Morvan, D., Calmonte, U., Charnley, S., et al. 2015, *SSRv*, 197, 47, doi: [10.1007/s11214-015-0156-9](https://doi.org/10.1007/s11214-015-0156-9)
- Brunetti, A., Sanchez del Rio, M., Golosio, B., Simionovici, A., & Somogyi, A. 2004, *Spectrochimica Acta Part B: Atomic Spectroscopy*, 59, 1725, doi: [https://doi.org/10.1016/j.sab.2004.03.014](https://doi.org/https://doi.org/10.1016/j.sab.2004.03.014)
- Clayton, R. N. 2002, *Nature*, 415, 860, doi: [10.1038/415860b](https://doi.org/10.1038/415860b)
- Cleeves, L. I., Bergin, E. A., Alexander, C. M. O. D., et al. 2014, *Science*, 345, 1590, doi: [10.1126/science.1258055](https://doi.org/10.1126/science.1258055)
- Cleeves, L. I., Bergin, E. A., Öberg, K. I., et al. 2017, *ApJL*, 843, L3, doi: [10.3847/2041-8213/aa76e2](https://doi.org/10.3847/2041-8213/aa76e2)
- Cleeves, L. I., Bergin, E. A., Qi, C., Adams, F. C., & Öberg, K. I. 2015, *ApJ*, 799, 204, doi: [10.1088/0004-637X/799/2/204](https://doi.org/10.1088/0004-637X/799/2/204)
- Cleeves, L. I., Loomis, R. A., Teague, R., et al. 2021, *ApJ*, 911, 29, doi: [10.3847/1538-4357/abe862](https://doi.org/10.3847/1538-4357/abe862)
- Cuzzi, J. N., & Zahnle, K. J. 2004, *ApJ*, 614, 490, doi: [10.1086/423611](https://doi.org/10.1086/423611)
- Dionatos, O., Woitke, P., Güdel, M., et al. 2019, *A&A*, 625, A66, doi: [10.1051/0004-6361/201832860](https://doi.org/10.1051/0004-6361/201832860)
- Donaldson, J. K., Weinberger, A. J., Gagné, J., et al. 2016, *ApJ*, 833, 95, doi: [10.3847/1538-4357/833/1/95](https://doi.org/10.3847/1538-4357/833/1/95)
- Du, F., Bergin, E. A., & Hogerheijde, M. R. 2015, *ApJL*, 807, L32, doi: [10.1088/2041-8205/807/2/L32](https://doi.org/10.1088/2041-8205/807/2/L32)
- Du, F., Bergin, E. A., Hogerheijde, M., et al. 2017, *ApJ*, 842, 98, doi: [10.3847/1538-4357/aa70ee](https://doi.org/10.3847/1538-4357/aa70ee)
- Dullemond, C. P., Juhasz, A., Pohl, A., et al. 2012, *RADMC-3D: A multi-purpose radiative transfer tool*. <http://ascl.net/1202.015>
- Favre, C., Cleeves, L. I., Bergin, E. A., Qi, C., & Blake, G. A. 2013, *ApJL*, 776, L38, doi: [10.1088/2041-8205/776/2/L38](https://doi.org/10.1088/2041-8205/776/2/L38)
- Furuya, K., & Aikawa, Y. 2014, *ApJ*, 790, 97, doi: [10.1088/0004-637X/790/2/97](https://doi.org/10.1088/0004-637X/790/2/97)
- Furuya, K., Aikawa, Y., Nomura, H., Hersant, F., & Wakelam, V. 2013, *ApJ*, 779, 11, doi: [10.1088/0004-637X/779/1/11](https://doi.org/10.1088/0004-637X/779/1/11)
- Furuya, K., Aikawa, Y., Sakai, N., & Yamamoto, S. 2011, *ApJ*, 731, 38, doi: [10.1088/0004-637X/731/1/38](https://doi.org/10.1088/0004-637X/731/1/38)
- Furuya, K., Drozdovskaya, M. N., Visser, R., et al. 2017, *A&A*, 599, A40, doi: [10.1051/0004-6361/201629269](https://doi.org/10.1051/0004-6361/201629269)
- Gaia Collaboration, Brown, A. G. A., Vallenari, A., et al. 2016, *A&A*, 595, A2, doi: [10.1051/0004-6361/201629512](https://doi.org/10.1051/0004-6361/201629512)
- Heays, A. N., Bosman, A. D., & van Dishoeck, E. F. 2017, *A&A*, 602, A105, doi: [10.1051/0004-6361/201628742](https://doi.org/10.1051/0004-6361/201628742)
- Herczeg, G. J., Linsky, J. L., Valenti, J. A., Johns-Krull, C. M., & Wood, B. E. 2002, *ApJ*, 572, 310, doi: [10.1086/339731](https://doi.org/10.1086/339731)
- Hogerheijde, M. R., Bergin, E. A., Brinch, C., et al. 2011, *Science*, 334, 338, doi: [10.1126/science.1208931](https://doi.org/10.1126/science.1208931)
- Huang, J., Andrews, S. M., Cleeves, L. I., et al. 2018, *ApJ*, 852, 122, doi: [10.3847/1538-4357/aaa1e7](https://doi.org/10.3847/1538-4357/aaa1e7)
- Kama, M., Bruderer, S., van Dishoeck, E. F., et al. 2016, *A&A*, 592, A83, doi: [10.1051/0004-6361/201526991](https://doi.org/10.1051/0004-6361/201526991)
- Krijt, S., Schwarz, K. R., Bergin, E. A., & Ciesla, F. J. 2018, *ApJ*, 864, 78, doi: [10.3847/1538-4357/aad69b](https://doi.org/10.3847/1538-4357/aad69b)
- Krot, A. N., Nagashima, K., Lyons, J. R., Lee, J.-E., & Bizzarro, M. 2020, *Science Advances*, 6, eaay2724, doi: [10.1126/sciadv.aay2724](https://doi.org/10.1126/sciadv.aay2724)
- Langer, W. D., Graedel, T. E., Frerking, M. A., & Armentrout, P. B. 1984, *ApJ*, 277, 581, doi: [10.1086/161730](https://doi.org/10.1086/161730)
- Lee, J.-E., Bergin, E. A., & Lyons, J. R. 2008, *Meteoritics and Planetary Science*, 43, 1351, doi: [10.1111/j.1945-5100.2008.tb00702.x](https://doi.org/10.1111/j.1945-5100.2008.tb00702.x)
- Lee, S., Nomura, H., Furuya, K., & Lee, J.-E. 2021, *ApJ*, 908, 82, doi: [10.3847/1538-4357/abd633](https://doi.org/10.3847/1538-4357/abd633)
- Loison, J.-C., Wakelam, V., Gratier, P., & Hickson, K. M. 2020, *MNRAS*, 498, 4663, doi: [10.1093/mnras/staa2700](https://doi.org/10.1093/mnras/staa2700)
- Loison, J.-C., Wakelam, V., Gratier, P., et al. 2019, *MNRAS*, 485, 5777, doi: [10.1093/mnras/stz560](https://doi.org/10.1093/mnras/stz560)
- Lyons, J. R., & Young, E. D. 2005, *Nature*, 435, 317, doi: [10.1038/nature03557](https://doi.org/10.1038/nature03557)
- Mangum, J. G., & Shirley, Y. L. 2015, *PASP*, 127, 266, doi: [10.1086/680323](https://doi.org/10.1086/680323)

- McMullin, J. P., Waters, B., Schiebel, D., Young, W., & Golap, K. 2007, in *Astronomical Society of the Pacific Conference Series*, Vol. 376, *Astronomical Data Analysis Software and Systems XVI*, ed. R. A. Shaw, F. Hill, & D. J. Bell, 127
- Miotello, A., Bruderer, S., & van Dishoeck, E. F. 2014, *A&A*, 572, A96, doi: [10.1051/0004-6361/201424712](https://doi.org/10.1051/0004-6361/201424712)
- Miotello, A., van Dishoeck, E. F., Kama, M., & Bruderer, S. 2016, *A&A*, 594, A85, doi: [10.1051/0004-6361/201628159](https://doi.org/10.1051/0004-6361/201628159)
- Mladenović, M., & Roueff, E. 2014, *A&A*, 566, A144, doi: [10.1051/0004-6361/201423733](https://doi.org/10.1051/0004-6361/201423733)
- . 2017, *A&A*, 605, A22, doi: [10.1051/0004-6361/201731270](https://doi.org/10.1051/0004-6361/201731270)
- Müller, H. S. P., Schlöder, F., Stutzki, J., & Winnewisser, G. 2005, *Journal of Molecular Structure*, 742, 215, doi: [10.1016/j.molstruc.2005.01.027](https://doi.org/10.1016/j.molstruc.2005.01.027)
- Müller, H. S. P., Thorwirth, S., Roth, D. A., & Winnewisser, G. 2001, *A&A*, 370, L49, doi: [10.1051/0004-6361:20010367](https://doi.org/10.1051/0004-6361:20010367)
- Nomura, H., Tsukagoshi, T., Kawabe, R., et al. 2021, arXiv e-prints, arXiv:2105.00976, <https://arxiv.org/abs/2105.00976>
- Öberg, K. I., van Broekhuizen, F., Fraser, H. J., et al. 2005, *ApJL*, 621, L33, doi: [10.1086/428901](https://doi.org/10.1086/428901)
- Qi, C., Wilner, D. J., Aikawa, Y., Blake, G. A., & Hogerheijde, M. R. 2008, *ApJ*, 681, 1396, doi: [10.1086/588516](https://doi.org/10.1086/588516)
- Roueff, E., Loison, J. C., & Hickson, K. M. 2015, *A&A*, 576, A99, doi: [10.1051/0004-6361/201425113](https://doi.org/10.1051/0004-6361/201425113)
- Sakamoto, N., Seto, Y., Itoh, S., et al. 2007, *Science*, 317, 231, doi: [10.1126/science.1142021](https://doi.org/10.1126/science.1142021)
- Schoonjans, T., Brunetti, A., Golosio, B., et al. 2011, *Spectrochimica Acta Part B: Atomic Spectroscopy*, 66, 776, doi: <https://doi.org/10.1016/j.sab.2011.09.011>
- Schroeder I, I. R. H. G., Altwegg, K., Balsiger, H., et al. 2019, *A&A*, 630, A29, doi: [10.1051/0004-6361/201833806](https://doi.org/10.1051/0004-6361/201833806)
- Schwarz, K. R., Bergin, E. A., Cleeves, L. I., et al. 2016, *ApJ*, 823, 91, doi: [10.3847/0004-637X/823/2/91](https://doi.org/10.3847/0004-637X/823/2/91)
- Shimajiri, Y., Kitamura, Y., Saito, M., et al. 2014, *A&A*, 564, A68, doi: [10.1051/0004-6361/201322912](https://doi.org/10.1051/0004-6361/201322912)
- Smith, R. L., Pontoppidan, K. M., Young, E. D., Morris, M. R., & van Dishoeck, E. F. 2009, *ApJ*, 701, 163, doi: [10.1088/0004-637X/701/1/163](https://doi.org/10.1088/0004-637X/701/1/163)
- Teague, R., Bae, J., Huang, J., & Bergin, E. A. 2019, *ApJL*, 884, L56, doi: [10.3847/2041-8213/ab4a83](https://doi.org/10.3847/2041-8213/ab4a83)
- Teague, R., Semenov, D., Guilloteau, S., et al. 2015, *A&A*, 574, A137, doi: [10.1051/0004-6361/201425268](https://doi.org/10.1051/0004-6361/201425268)
- Tenner, T. J., Ushikubo, T., Nakashima, D., et al. 2018, *Oxygen Isotope Characteristics of Chondrules from Recent Studies by Secondary Ion Mass Spectrometry*, ed. S. S. Russell, J. Connolly, Harold C., & A. N. Krot, 196–246, doi: [10.1017/9781108284073.008](https://doi.org/10.1017/9781108284073.008)
- Tielens, A. G. G. M. 2005, *The Physics and Chemistry of the Interstellar Medium*
- van der Tak, F. F. S., Black, J. H., Schöier, F. L., Jansen, D. J., & van Dishoeck, E. F. 2007, *A&A*, 468, 627, doi: [10.1051/0004-6361:20066820](https://doi.org/10.1051/0004-6361:20066820)
- van Dishoeck, E. F., Kristensen, L. E., Mottram, J. C., et al. 2021, *A&A*, 648, A24, doi: [10.1051/0004-6361/202039084](https://doi.org/10.1051/0004-6361/202039084)
- Visser, R., van Dishoeck, E. F., & Black, J. H. 2009, *A&A*, 503, 323, doi: [10.1051/0004-6361/200912129](https://doi.org/10.1051/0004-6361/200912129)
- Wilson, T. L. 1999, *Reports on Progress in Physics*, 62, 143, doi: [10.1088/0034-4885/62/2/002](https://doi.org/10.1088/0034-4885/62/2/002)
- Woods, P. M., & Willacy, K. 2009, *ApJ*, 693, 1360, doi: [10.1088/0004-637X/693/2/1360](https://doi.org/10.1088/0004-637X/693/2/1360)
- Yamamoto, D., Kuroda, M., Tachibana, S., Sakamoto, N., & Yurimoto, H. 2018, *ApJ*, 865, 98, doi: [10.3847/1538-4357/aadcee](https://doi.org/10.3847/1538-4357/aadcee)
- Yurimoto, H., & Kuramoto, K. 2004, *Science*, 305, 1763, doi: [10.1126/science.1100989](https://doi.org/10.1126/science.1100989)
- Zhang, K., Bergin, E. A., Blake, G. A., Cleeves, L. I., & Schwarz, K. R. 2017, *Nature Astronomy*, 1, 0130, doi: [10.1038/s41550-017-0130](https://doi.org/10.1038/s41550-017-0130)
- Zhang, K., Bergin, E. A., Schwarz, K., Krijt, S., & Ciesla, F. 2019, *ApJ*, 883, 98, doi: [10.3847/1538-4357/ab38b9](https://doi.org/10.3847/1538-4357/ab38b9)